Impacts of Typhoon Track and Island Topography on the Heavy Rainfalls in Taiwan Associated with Morakot (2009)

BAOGUO XIE

Laboratory for Climate and Ocean-Atmosphere Studies, Department of Atmospheric and Oceanic Sciences, Peking University, Beijing, China, and Department of Meteorology, The Pennsylvania State University, University Park, Pennsylvania

FUQING ZHANG

Department of Meteorology, The Pennsylvania State University, University Park, Pennsylvania

(Manuscript received 20 September 2011, in final form 13 April 2012)

ABSTRACT

Cloud-resolving ensemble simulations and sensitivity experiments utilizing the Weather Research and Forecasting model (WRF) are performed to investigate the dynamics and predictability of the record-breaking rainfall and flooding event in Taiwan induced by Typhoon Morakot (2009). It is found that a good rainfall forecast foremost requires a good track forecast during Morakot's landfall. Given a good track forecast, interaction of the typhoon circulation with complex topography in southern Taiwan plays a dominant role in producing the observed heavy rainfalls. The terrain slope, strength of the horizontal winds, and mid–lower-tropospheric moisture content in the southwesterly upslope flow are the primary factors that determine the rainfall location and intensity, as elucidated by the idealized one-dimensional precipitation-rate forecast model. The typhoon circulation and the southwesterly monsoon flow transport abundant moisture into southern Taiwan, which produces the heavy rainfall through interactions with the complex high terrain in the area. In the meantime, as part of the south China monsoon, the southwesterly flow may be substantially enhanced by the typhoon circulation.

1. Introduction

Rainfall and the subsequent flooding produced by tropical cyclones (TCs) is a significant natural hazard, especially for coastal communities. On average, three–four typhoons hit the island of Taiwan every year. As a result of the island's topography, specifically the Central Mountain Range (CMR), Taiwan suffers from heavy rains and flood disasters caused by TCs each year. Because of the complex topographic features and their interactions with TCs, it is extremely hard to predict the track, intensity change, and precipitation of TCs as they approach land (Yeh and Elsberry 1993; Wu and Kuo 1999; Wu 2001; Jian and Wu 2008). The predictability of rainfall associated with TCs is strongly dependent on an accurate forecast of the TC track, which may be significantly deflected by the complex high topography. Previous studies with numerical model simulations demonstrated that the CMR could alter TC structure, intensity, and rainbands and could also induce a low-level jet (LLJ) that has an important impact on low-level convergence and the upstream water vapor supply (e.g., Chang 1982; Chang et al. 1993; Lin 1993; Lin et al. 1999, 2001; Chiao and Lin 2003; Kuo and Wang 1997; Wu et al. 2002, 2009; Fang et al. 2011). Moreover, this is also the region where the TC circulations usually interact with the South China Sea summer monsoon. The southwesterly monsoon flow is believed to be responsible for supplying large amounts of moisture to the TC environments during the monsoon season (e.g., Chiao and Lin 2003; Wu et al. 2009; Ge et al. 2010; Hong et al. 2010; Wu et al. 2011; Liang et al. 2011; Nguyen and Chen 2011; Chien and Kuo 2011). However, the specific role the monsoon plays in the heavy rainfall is difficult to elucidate since the monsoon is a large-scale system, acting as a background environment. It remains unclear whether the TCs influence the monsoon gyres over this region that subsequently affect the rainfall location and intensity.

Corresponding author address: Dr. Fuqing Zhang, Department of Meteorology, The Pennsylvania State University, University Park, PA 16802.
E-mail: fzhang@psu.edu

DOI: 10.1175/MWR-D-11-00240.1

The current study seeks to further understand the dynamics and predictability of the record-breaking rainfall and flooding event in Taiwan induced by Typhoon Morakot (2009). It is an extension of a recent study that examined the predictability of Morakot with a cloud-resolving ensemble [Zhang et al. 2010 (Z10)] and is complementary to Fang et al. [2011 (F11)], which also examined the impact of the CMR on the extreme rainfall of this event. In Z10, the high-resolution convection-permitting mesoscale ensemble, initialized with analysis and flow-dependent perturbations obtained from a real-time global ensemble data assimilation (EDA) system, was found to be able to predict this record-breaking rainfall event, producing probability forecasts potentially valuable to the emergency management decision makers and the general public. Through sensitivity experiments performed by removing the terrain of Taiwan, F11 found that the orography is crucial in determining the structure, intensity, and variability of Morakot's rainfall. Consistent with Z10, they concluded that the forecasting of extreme rainfall events such as Morakot would benefit from probabilistic prediction provided by a high-resolution mesoscale ensemble forecast system.

The primary focuses of the current study are 1) the relationship between predictability of the typhoon track and precipitation, 2) the enhancement of orographically induced rainfall, and 3) the interactions between the southwest monsoon and Morakot. Section 2 describes the model configuration and experimental design. Section 3 presents an overview of Morakot and the performance of the Weather Research and Forecasting model (WRF) control and reference simulations. Section 4 examines the sensitivity of typhoon-associated rainfall in Taiwan to track predictability. The effects of island topography on rainfall predictability are presented in section 5. Section 6 documents the interactions between the typhoon circulation and the southwest monsoon, while concluding remarks are given in section 7.

2. The forecast model

The Weather Research and Forecasting model developed at the National Center for Atmospheric Research (Skamarock et al. 2007) is used in this study. The model setup is the same as in Z10. All simulations have 2 two-way-nested model domains with grid spacings of 13.5 km (D1) and 4.5 km (D2), respectively, and 34 levels in a stretched vertical coordinate. Each domain has 603 (540) grid points in the west–east (south–north) direction covering an area ranging from 98° to 177°E and 7°S to 44°N for D1 and from 113° to 135°E and 13° to 35°N for D2 (Fig. 1). Initial conditions are from an

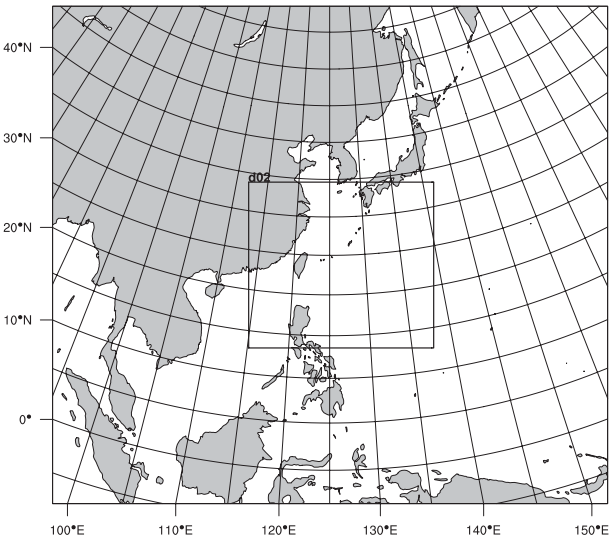

FIG. 1. Model domain configuration. The domain sizes are both 603 (west–east) by 540 (south–north) grid points with a horizontal grid spacing of 13.5 km (4.5 km) for the coarse (fine) domain.

experimental real-time global ensemble data assimilation system with 60 ensemble members that represent the flow-dependent analysis uncertainty of the global EDA system described in detail in Z10. The EDA system is initiated at 0000 UTC 5 August and runs for 132 h, ending at 1200 UTC 10 August. The WRF Single-Moment 6-class (WSM6) graupel microphysics scheme (Hong and Lim 2006) is used and no cumulus parameterization scheme is utilized in these experiments. The deterministic WRF forecast initialized at 0000 UTC 5 August with the EDA analysis (experiment IC_EDA_DF in Z10) is relabeled as the control run (hereafter referred to as CNTL00). Three members (15, 23, and 54 or CNTL15, CNTL23, and CNTL54) from the ensemble forecast of Z10 will also be used as reference runs for different sensitivity experiments. Given the very specific spatial and temporal distribution of the heavy precipitation from Morakot as demonstrated in Z10 and F11, members 15 and 23 were selected as additional reference simulations to augment the CNTL00 forecasts, as both ensemble members provided simulated precipitation distributions that were similar to the control and to the actual spatial and temporal variations. Member 54 is chosen as a counterexample for terrain sensitivity because its track deviated too far to the north and completely missed a landfall in Taiwan, resulting in nearly no precipitation over Taiwan.

The observed track and intensity data are obtained from the Joint Typhoon Warning Center (JTWC). The Final Operation Global (FNL) analysis data from the National Centers for Environmental Prediction (NCEP) are used for synoptic analysis and comparison with model simulations.

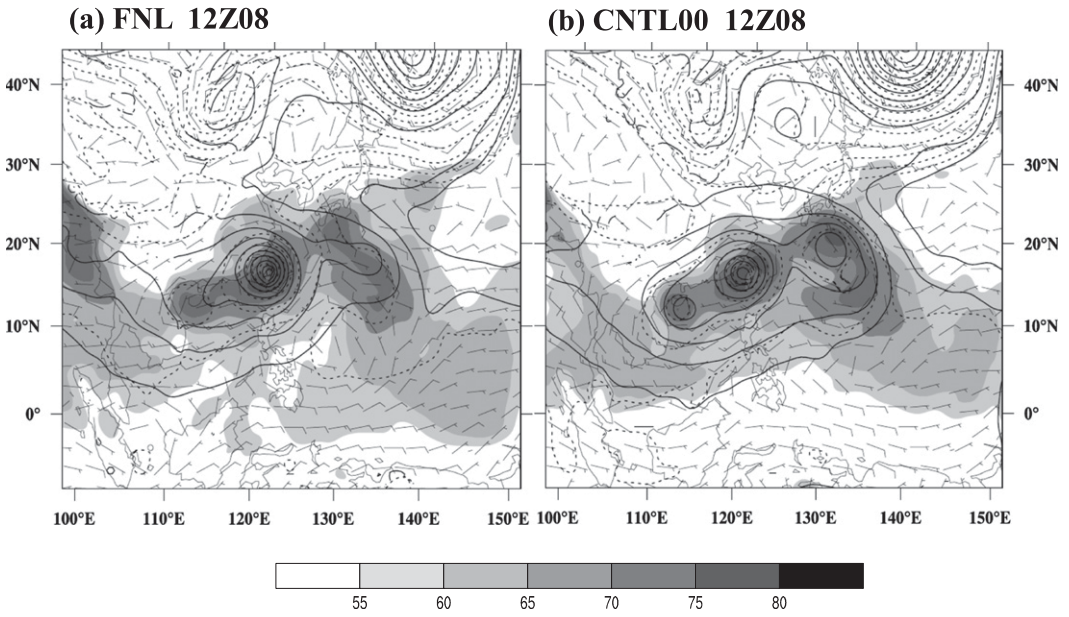

FIG. 2. The 850-hPa wind (full wind barb is 10 m s^{-1}) and geopotential height (solid contour lines; from 1150 to 1530 m by every 40 m), 500-hPa height (dashed contour lines; from 5440 to 5880 m by every 40 m), and precipitable water (shaded; kg m^{-2}) for the (a) FNL analysis and (b) CNTL00 forecast valid at 1200 UTC 8 Aug 2009.

3. Overview of Morakot and performance of the WRF control and reference simulations

Morakot is the deadliest typhoon to hit Taiwan in recorded history. It caused catastrophic damage by way of more than 700 fatalities and ~$3.3 billion (USD) in property damages. Morakot's effects on Taiwan lasted from 6 to 10 August, even though the storm made landfall at 1800 UTC 7 August in south Taiwan (Hong et al. 2010). Despite only having the intensity of a category-2 storm, Morakot brought record-breaking rainfall with 2777 mm in 72 h (Z10). Morakot formed on 2 August 2009 as a tropical depression within a monsoon trough. It gradually intensified to a typhoon on 5 August while moving westward toward Taiwan. The storm attained its peak strength on 7 August with a central pressure of ~945 hPa before making landfall on the mideast coast of Taiwan Island. The strongest rainfall occurred between 0000 UTC 8 August and 0000 UTC 9 August (Z10; Hong et al. 2010; F11). For synoptic analysis, the 850-hPa geopotential height and winds, the 500-hPa geopotential height, and precipitable water (PW) at 1200 UTC 8 August are plotted in Fig. 2a using the FNL analysis. There is very high precipitable water (80 kg m^{-2}) throughout the region that is associated with the combined effects of Morakot and the southwest monsoon. The southwest monsoon flow established a strong water vapor channel to the typhoon during the most intense precipitation period. There is also strong low-level jet in this region seen from the 850-hPa wind field. Meanwhile, there was another tropical storm that formed to the west of Morakot, which may have had a limited influence on Morakot. Based on the landfall location and the size (~800-km radius) of Morakot (Fig. 2a), the outer circulation in southwestern Taiwan impinged on the slope side of the southern part of the CMR, and the slope of the mountain helped to create strong updrafts. This may have been the primary reason for the record flooding and will be the focus of this study in the following sections. After departing Taiwan Island, Morakot weakened to a severe tropical storm before making its second landfall on mainland China, and then gradually dissipated while moving farther inland on 11 August.

In comparison with the synoptic analysis, Fig. 2b contains the 850-hPa geopotential height and winds and the 500-hPa geopotential height and precipitable water at 1200 UTC 8 August as forecasted by CNTL00. Very high PW content with values exceeding 80 kg m^{-2} is forecasted in both the southwest and southeast quadrants of Morakot, which is consistent with the FNL analysis (Fig. 2a). A subtropical high pressure system to the north of Morakot and the LLJ associated with the southwest monsoon were also well captured in the CNTL00 simulation, though the CNTL00- (and ensemble) simulated Morakot may be somewhat smaller in size (refer to Fig. 4 in Z10). The cyclone-scale circulation and the environmental flow patterns are also well forecasted by two of the best performing members of the Z10 ensemble (CNTL15 and CNTL23; figures not shown).

CNTL00, CNTL15, and CNTL23 also effectively simulated the track before and during the landfall in Taiwan. Despite noticeable track errors while Morakot moved toward Taiwan, the forecasted Morakot in all three experiments made landfall within 25 km of the observed location (Fig. 3a). The sharp northward turning of the observed track after landfall in Taiwan is also captured by all three experiments, with CNTL23 being the most accurate. Despite a low bias at the initial time and high bias at the time of peak intensity, all three experiments forecasted the observed typhoon intensity reasonably well in terms of the maximum surface wind (Fig. 3b). However, all three experiments persistently underpredicted the storm's intensity in terms of the minimum sea level pressure (Fig. 3c). The reasons for the mismatch between wind and pressure are complex and likely related to the deficiencies in the forecast model, which is beyond the scope of the current study.

The observational gridded analysis of the 72-h accumulated rainfall (from 0000 UTC 6 August to 0000 UTC 9 August) associated with Typhoon Morakot in Taiwan mainly occurred in southern Taiwan, with a maximum of 2410 mm in the gridded analysis provided by the Central Weather Bureau of Taiwan (Fig. 4a). The location of the heaviest total rainfall and rainfall intensity over southern Taiwan is also reasonably well forecasted by all three simulations. Nevertheless, each forecast has a few apparent shortcomings. The peak rainfall value in CNTL15 is 1851 mm (Fig. 4c), which is an underestimation, while both CNTL00 and CNTL23 considerably overestimate the peak rainfall with maximum values of 3545 (Fig. 4b) and 2920 mm (Fig. 4d), respectively. The heaviest rainfall region in both CNTL00 and CNTL15 was biased more to the south than observed, which is likely due to a southwestward track error of the simulated storm during its crossing over Taiwan in both experiments.

Another reference simulation comes from ensemble CNTL54, whose track forecast was so far north that the simulated storm completely missed the landfall in Taiwan (Fig. 3a). Consequently, the maximum 72-h forecasted accumulated rainfall over Taiwan by CNTL54 was less than 500 mm (Fig. 4i), which was less than one-fifth of the observed peak value. Compared to CNTL00, CNTL15, and CNTL23, this member is also slightly weaker in intensity for both maximum surface wind (Fig. 3b) and minimum sea level pressure (Fig. 3c).

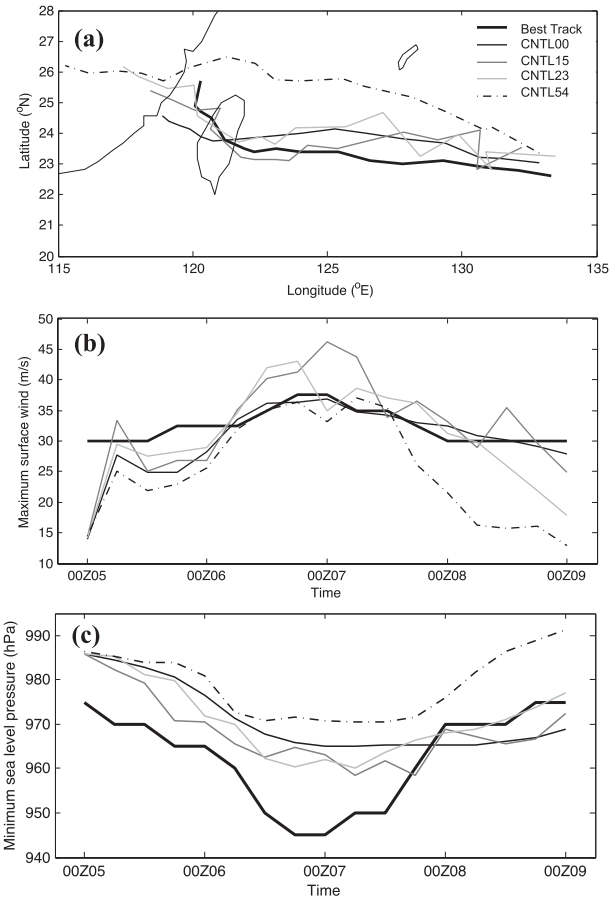

FIG. 3. The (a) 72-h forecasted track, (b) minimum sea level pressure, and (c) maximum surface wind for observations, CNTL00, CNTL15, CNTL23, and CNTL54.

4. Sensitivity of the rainfall to Morakot's track

a. Ensemble-based analysis

The importance of Morakot's track for the predictability of the heavy rainfall over Taiwan can first be inferred from the ensemble prediction of Z10 that found that the members with good track forecasts also produced good rainfall forecasts. This can be further quantified by examining the correlation between the forecast errors in the storm's position and the associated rainfall based on the ensemble analysis. To quantitatively determine the difference between the observations and each member, the normalized absolute precipitation error (NAPE) is defined as

$$\mathrm{NAPE} = \frac{1}{N}\sum_{i=1}^{N}\frac{|R_i - R_i^o|}{\max(R_i, R_i^o)}, \qquad (1)$$

where N is the total number of grid points with precipitation in either the observation and/or the simulation, R_i is the precipitation in an ensemble member, and R_i^o is the precipitation in an observation, respectively. A smaller value of NAPE indicates a better forecast of precipitation. The correlation between NAPE and the track error (distance between the positions of the

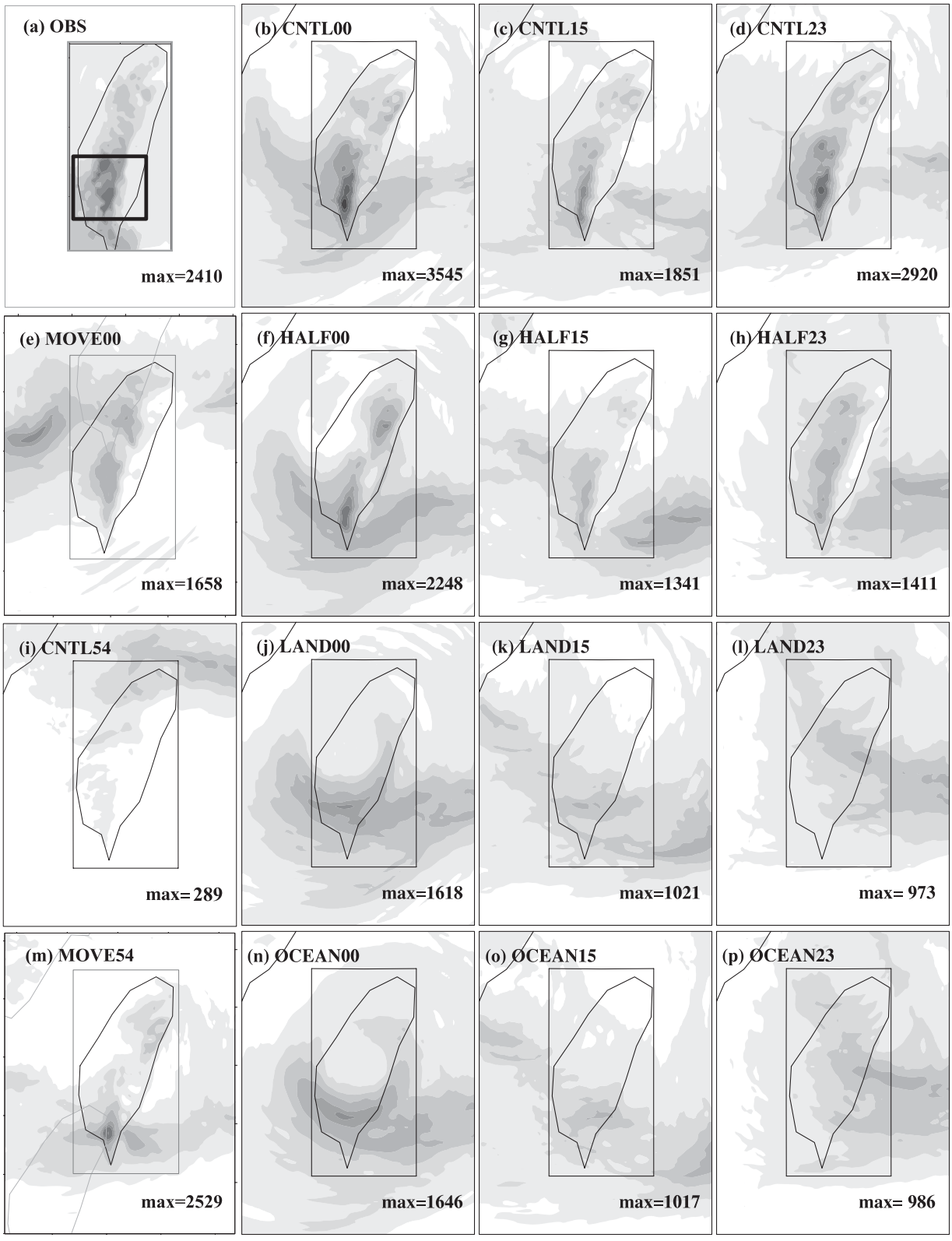

FIG. 4. The 72-h (from 0000 UTC 6 Aug to 0000 UTC 9 Aug) accumulated rainfall (shaded; mm) of Typhoon Morakot over Taiwan from (a) observations, (b)–(d),(i) CNTL simulations, and (e)–(h),(j)–(p) other experiments as indicated. The rectangular box in (a) indicates the heavy rainfall region.

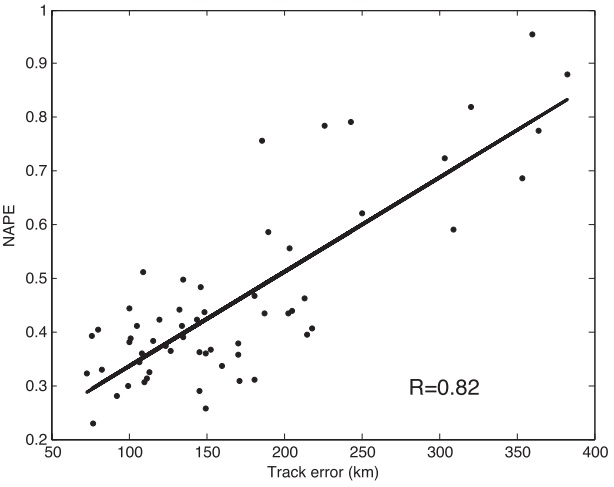

FIG. 5. Scatterplot of normalized absolute 72-h accumulated precipitation error against the track error (averaged from the 3-h priori and posterior to the landfall time) of each member.

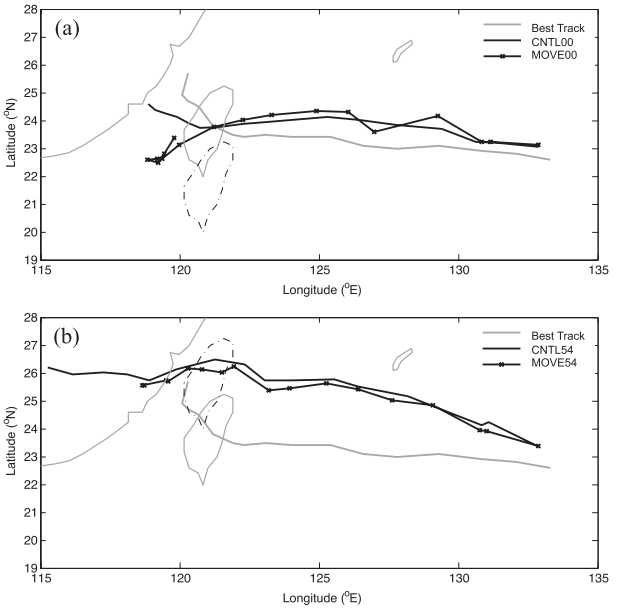

FIG. 6. The 72-h forecasted tracks of (a) MOVE00 and (b) MOVE54. The dashed coastlines of Taiwan indicate the moved terrain.

ensemble member and best-track observations) averaged from the 3-h a priori and posterior to landfall time is as large as 0.82 (significant at the 95% confidence level; Fig. 5), suggesting that the accuracy of the quantitative precipitation forecast (QPF) for Morakot is closely related to the predictability of its track.

The QPF dependence on track is also demonstrated in Figs. 4a–d, which show 72-h accumulated rainfall from observations as well as cases that provided the best tracks. Aside from CNTL00, which is the forecast from the ensemble mean, CNTL15 and CNTL23 are among the best performing ensemble members with the smallest track errors, and both also produce very good rainfall forecasts. In particular, with a good track forecast, CNTL23 produced a rainfall forecast close to observations in terms of both location and intensity (Fig. 4d). CNTL54, on the other hand, completely misses the landfall in Taiwan by taking a far more northward track and thus produces minimum precipitation over southern Taiwan in the observed flooding area (Fig. 4i).

b. Sensitivity experiment of moved terrain

To further elucidate the dependence between Morakot's track and rainfall forecasts, two sensitivity experiments (MOVE00 and MOVE54) are performed. These experiments examine the sensitivity of rainfall to track forecasting by artificially relocating the island in the simulation of CNTL00 (CNTL54), which has a good (poor) QPF forecast. MOVE00 relocates Taiwan Island south of its original location by 160 km such that the track of the simulated typhoon will be to the far north of the island, which results in a missed landfall on Taiwan; it can therefore be easily compared to some members in the ensemble with erroneous northward track errors in Z10 (such as CNTL54). MOVE54, on the other hand, relocates the island north of its original location by 200 km, such that the simulated typhoon will make direct landfall and cross over the island as in the observations (or CNTL00, CNTL15, and CNTL23). In both MOVE00 and MOVE54, the ''atmosphere'' originally occupied by the mountains was extrapolated directly from the full pressure-level data already available in the global model at initialization. We assigned a sea surface temperature (SST) in place of the original island by extrapolating the SST from nearby.

The track differences between CNTL00 and MOVE00 are shown in Fig. 6a (dashed coastline denotes the moved terrain). MOVE00 has approximately the same track as CNTL00 before 1800 UTC 7 August (landfall time), but turns noticeably more southwestward than CNTL00 thereafter, implying that the typhoon track may be modulated by the typhoon–terrain interaction. With the relocated island and thus missed landfall, the precipitation in MOVE00 is greatly reduced, with a maximum 72-h accumulated rainfall of 1658 mm, while the peak rainfall is located in the northern part of the moved island (Fig. 4e). On the other hand, to compensate for the track error that led to the missed landfall in CNTL54, MOVE54 relocates Taiwan Island 200 km to the north of its natural position, which could have additional impacts on the resulting precipitation. In this case, the difference between the tracks with and without the moved terrain is

small preceding landfall (Fig. 6b), and the simulated Morakot in MOVE54 makes landfall on the relocated island at approximately the same location as the observed track (with respect to the island terrain). However, the speed of the simulated Morakot in MOVE54 is much slower when passing over Taiwan, which again indicates the influence of the interaction between the typhoon and the topography on its track since there is no noticeable difference in the monsoon flow with the relocation of Taiwan's terrain. In MOVE54, the maximum rainfall center is located farther south and the rainfall exceeded 2529 mm (Fig. 4m), which is greatly enhanced over the reference run of CNTL54 (and close to the observed maximum). This again highlights the importance of track forecast accuracy, as well as Taiwan's topography, to the accuracy of the quantitative precipitation forecast.

5. Orographic precipitation enhancement

a. No-terrain experiments

The dependence between precipitation associated with Morakot in Taiwan and the maximum rainfall located along the slope of the CMR suggests that the interaction between Morakot and the CMR is critical in this flooding event. A series of sensitivity experiments are therefore conducted to examine the sensitivity of rainfall to the terrain of Taiwan.

The first sets of experiments (OCEAN00, OCEAN15, and OCEAN23) are conducted in the same way as in CNTL00, CNTL15, and CNTL23, but the topography is completely removed by changing the land surface to ocean (similar sensitivities are also performed in F11). The space originally occupied by Taiwan's terrain is now filled by the data extrapolated from the global analysis. Even with the absence of mountains and land, the maximum 72-h accumulated rainfall of OCEAN00 (Fig. 4n) is 1646 mm, which is about 45% of the peak rainfall in CNTL00 (Fig. 4b). The heaviest rainfall area is also located in the southern part of Taiwan but extends more to the west and east (along the south side of the primary typhoon circulation) than the more north–south orientation in CNTL00 (because of the interaction with the CMR). The rainfall simulated in OCEAN00 implies that Morakot brings extremely heavy and asymmetrically distributed rainfall to Taiwan Island even if there is no topography or land. Similar changes in the distribution of the rainfall are observed in OCEAN15 and OCEAN23, though the peak values of rainfall in these two experiments are considerably smaller (Figs. 4o,p). These results are consistent with F11, which also showed great rainfall reduction without Taiwan topography.

What causes the asymmetry in the rainfall distribution in the absence of topography on Taiwan? First examined is the impact of vertical wind shear, which can often make the rainfall around a TC highly asymmetric. Past studies have shown that the vertical wind shear can influence the storm motion and the distribution of associated convection (Corbosiero and Molinari 2002, 2003; Cecil 2007; Gao et al. 2009). The rainfall may also appear more substantial on the downshear left if the falling hydrometers in this sector are advected by the TC's cyclonic circulation (e.g., Frank and Ritchie 1999). Figures 7a, b show the vertical wind shear (difference between the 200- and 700-hPa winds) along with the storm motion vector and the 3-h accumulated rainfall for OCEAN00 at 0000 and 0006 UTC 8 August, respectively. It is seen that although the rainfall is located around the symmetric circulation of the eyewall and in the outer rainband area, the maximum rainfall occurs at the downshear left (south) side of the typhoon. This finding is consistent with previous studies about TC inner-core-induced rainfalls in a sheared environment (Corbosiero and Molinari 2002; Cecil 2007). In a diabatic environment with strong latent heat release, the low-level negative vorticity advection and the upper-level divergence could be balanced by the storm-relative flow on the downshear side (Wang and Holland 1996; Bender 1997; Frank and Ritchie 1999; Wu et al. 2006; Braun and Wu 2007). If the cyclone moves in a unidirectionally sheared environment with the ambient flow, there will be inward and outward storm-relative flow at low levels and upper levels on the downshear side, respectively. This process will produce negative (positive) vorticity advection at the low (upper) levels. Because of the vorticity conservation constraint, the negative (positive) vorticity advection will be balanced by vortex stretching (shrinking). Consequently, a deep layer of upward motion on the downshear side of the vortex will appear. As seen in Figs. 7c,d, the Taiwan topography has little impact on the vertical wind shear at these two times but the storm's forward motion has slowed in CNTL00. Another factor that influences the maximum rainfall toward the south of the typhoon circulation may be the interaction of the typhoon circulation with the southwesterly summer monsoon circulation (and the corresponding asymmetry in moisture distribution; e.g., Fig. 2) that meets Morakot at the south and southwest side. This factor has been recently explored in great detail in Wu et al. (2011) and Liang et al. (2011) and will be revisited in section 6.

Other experiments (LAND00, LAND15, and LAND23) are performed in a manner that is similar to OCEAN00, OCEAN15, and OCEAN23, but instead of replacing the island with the ocean surface, the topography is removed and a flat island with no elevation is utilized. The resulting rainfall forecasts (Figs. 4j–l) from each of

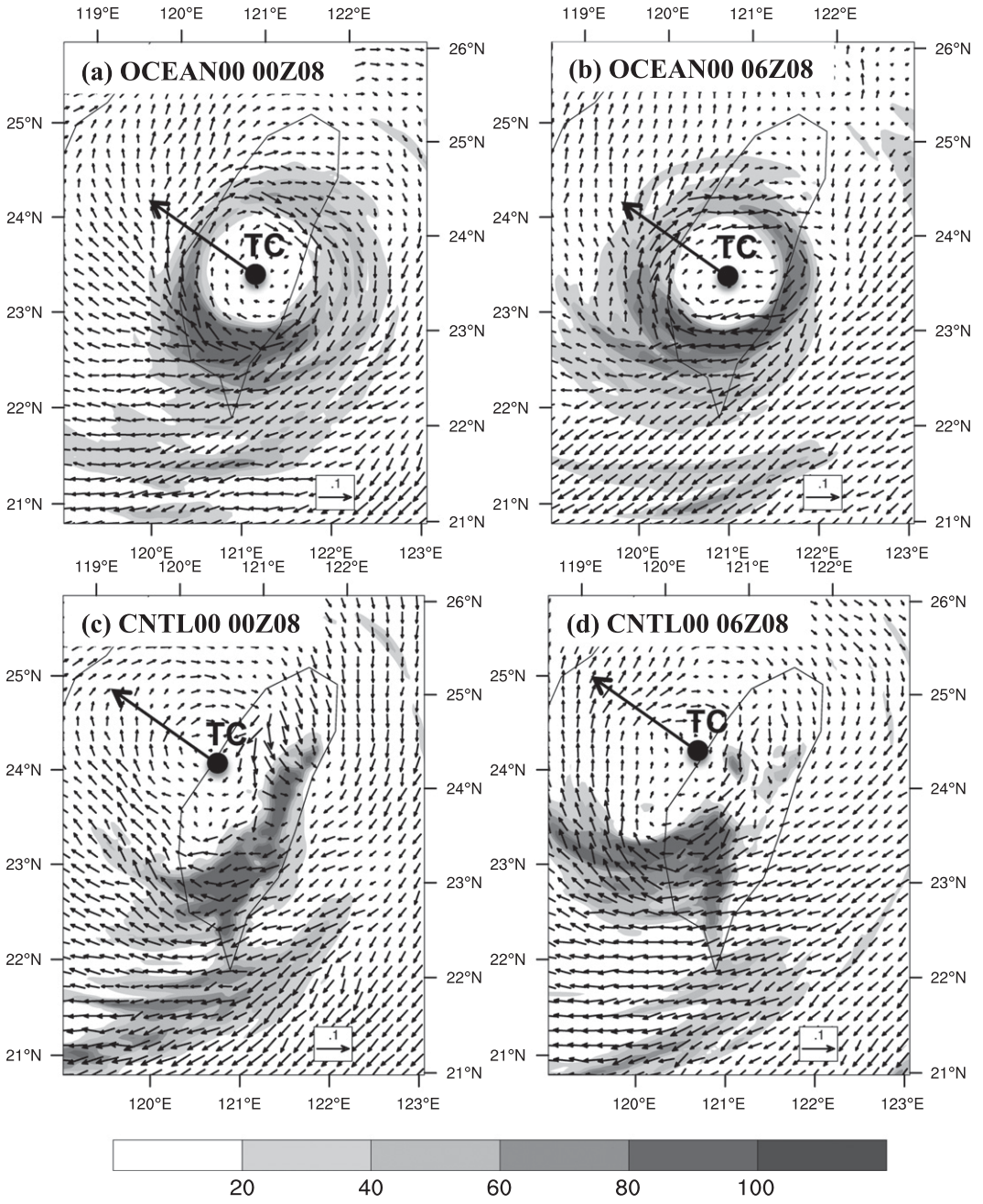

FIG. 7. The vertical wind shear (vector; m s^{-1} hPa^{-1}) between 200 and 700 hPa, and the 3-h accumulated rainfall (shaded; mm) of (a),(b) OCEAN00 and (c),(d) CNTL00 at 0000 and 0600 UTC 8 Aug, respectively. Solid dots and arrows indicate the simulated center and moving direction of Morakot, respectively.

the flat-island experiments are similar to their respective no-island runs, implying that it is primarily the island topography, not the land interaction that causes the redistribution of the rainfall. As a consequence, the flat-island and no-island experiments produced similar amounts of precipitation when averaged over the southern part of the island, both of which were considerably smaller amounts than the full-terrain experiments (Fig. 8b). On the other hand, when the rainfall was averaged over the entire 4.5-km nested domain, experiments with and without the island topography produced nearly equal amounts of precipitation (Fig. 8a). In conclusion, the presence of Taiwan Island leads to the redistribution of rainfall over elevated terrain, but does not necessarily extract more water from the atmosphere.

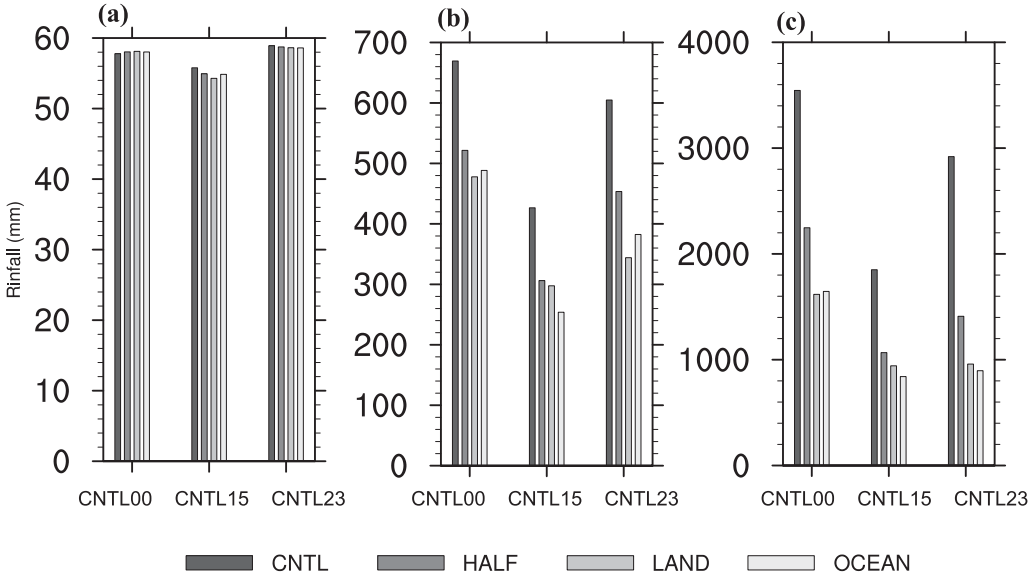

FIG. 8. The 72-h average rainfall (a) in the inner domain and (b) over Taiwan, and (c) maximum rainfall of four experiments (CNTL, HALF, LAND, and OCEAN) for CNTL00, CNTL15, and CNTL23.

b. Sensitivity to terrain height

Given the sharp contrast in the rainfall distributions between the experiments with and without Taiwan Island, it is obvious that the island topography plays a major role in the record-breaking rainfall in southern Taiwan and along the CMR. To further examine the effect of the terrain, the experiments HALF00, HALF15, and HALF23 are performed in a similar way to CNTL00, CNTL15, and CNTL23 except that all the terrain elevations in Taiwan are reduced by 50%. As in the flat-island and no-island experiments, the nested-domain-averaged precipitation in each of the reduced-terrain experiments is nearly the same as in the full-terrain experiments (Fig. 8a). On the other hand, each of the half-terrain experiments has ~30% lower total precipitation than the full-terrain runs when averaged over the island (Fig. 8b). Compared with the flat-terrain experiments, the half-terrain rainfall is about 10% larger for HALF00 and only 3% larger for HALF15 but greater than 30% larger for HALF23, suggesting that the impact of the topography by no means has a linear relationship to the terrain heights or terrain slopes, even if the rainfall is only averaged over the island where the terrain heights are changed.

The nonlinearity with respect to the height changes is even more apparent in the peak values of rainfall in each set of experiments. The maximum rainfall for the half-terrain-height experiments is 2247 mm for HALF00 (Fig. 4f), 1067 mm for HALF15 (Fig. 4g), and 1410 mm for HALF23 (Fig. 4h), which is reduced by 36%, 42%, and 51% when compared with the full-terrain (CNTL) simulations (Fig. 8c). On the other hand, the rainfall distribution in the half-terrain-height experiments is similar to the full-terrain control runs with peak rainfall located in southern Taiwan along the western slope of the CMR.

To further examine the impact of terrain height and slope, Figs. 9a–c show the meridional mean of the 72-h accumulated rainfall distribution (along with the mean terrain heights) averaged over the heavy rainfall region in Taiwan Island from both the full-terrain (CNTL) experiments and the reduced-terrain (HALF) experiments. On average, for both sets of experiments, the rainfall increases gradually on the west (windward) side of the CMR with terrain heights (as well as with the terrain slope; not shown) until it reaches a maximum at ~20 km west of the averaged terrain peak. The rainfall then decreases sharply eastward from across the peak to the eastern lee slope of the CMR. Reducing the terrain height by half will greatly reduce the rainfall amount in the windward side of the CMR (Figs. 9e,f); the larger the original rainfall amount, the more it will be reduced by the reduced terrain heights (DIFF1 denotes the difference between HALF and LAND, and DIFF2 the difference between HALF and CNTL). To the east side of the CMR, the change in rainfall with reduced terrain height in each pair of the CNTL–HALF experiments is smaller and less systematic. These relationships are further verified in Figs. 10a–c, which show scatterplots of the rainfall reduction (between CNTL and HALF) versus the rainfall in CNTL at all model grid points over Taiwan. The rainfall reduction is highly correlated with the original rainfall amount in each pair of the experiments, with the correlation as high as

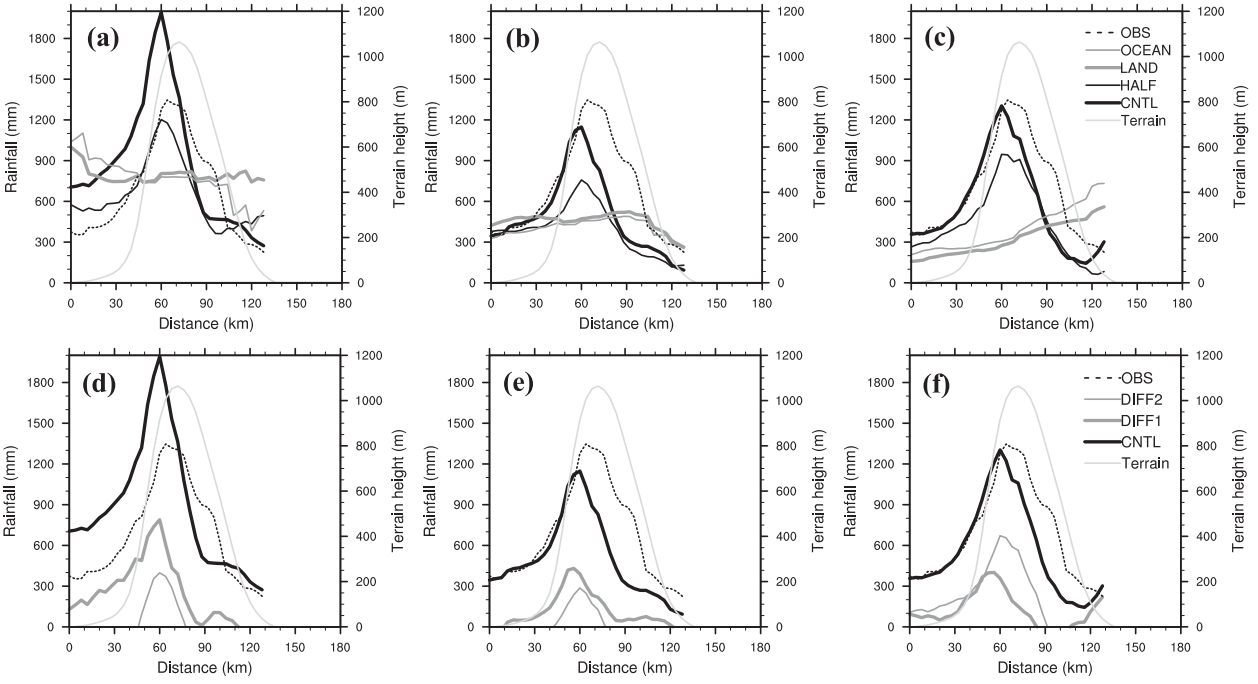

FIG. 9. The meridionally averaged 72-h accumulated rainfall distribution in a west–east direction across Taiwan for CNTL (thick black solid line) and HALF (thin black solid line) of (a) CNTL00, (b) CNTL15, and (c) CNTL23. The difference between the rainfall of LAND and OCEAN (DIFF1) and the difference between rainfall of HALF and LAND (DIFF2) for (d) CNTL00, (e) CNTL15, and (f) CNTL23. The gray lines corresponding with the right axis indicate terrain height. Observed rainfall (dashed lines) is also shown in each panel for reference.

0.64, 0.87, and 0.71, respectively (Figs. 10a–c). Though to a slightly lesser degree, similar relationships between rainfall reduction and the original rainfall amount can also be found between the flat terrain and the terrains in HALF (Figs. 10d–f). Note that the correlation coefficients estimated here include both windward and leeward rainfall but the correlations are nearly unchanged if only the windward points are used (not shown). Given that LAND and OCEAN do not have terrain, the precipitation differences between the two experiments are not only smaller, but less correlated with the raw LAND data (Figs. 10g–i).

c. *Terrain effects explained by a 1D model*

The one-dimensional (1D) model proposed by Smith (1979) is used to examine the essential factors in the strong orographic precipitation associated with Typhoon Morakot. Assuming an air parcel of unit volume at height z in a saturated region of the atmosphere, the condensation rate in the volume $D\rho_{w_s}/Dt$ is determined by the decreasing rate of saturated water vapor density ($\rho_{w_s} = r_s\rho_{\text{air}}$), which can be approximated by adiabatic lifting as

$$\frac{D\rho_{w_s}}{Dt} = -\left.\frac{d\rho_{w_s}}{dz}\right|_{\text{ad}} w. \tag{2}$$

If the raindrops can form immediately from the cloud droplets and the hydrometeors fall directly to the ground with no downwind drift, then the rate of precipitation at the ground is the vertical integral of (2):

$$R = -\int_0^\infty w\left.\frac{d\rho_{w_s}}{dz}\right|_{\text{ad}} dz, \tag{3}$$

where the intensity of orographic lifting can be estimated by assuming the flow is proportional to the slope of the mountain surface:

$$w = \mathbf{V}\cdot\mathbf{S}, \tag{4}$$

where $\mathbf{V}$ is the horizontal wind and $\mathbf{S}$ is the terrain slope (defined as the gradient of the mountain height ∇H).

To simplify this case, we assume that the environmental temperature lies along a moist adiabat, so that

$$\left.\frac{d\rho_{w_s}}{dz}\right|_{\text{ad}} = \frac{d\rho_{w_s}}{dz}. \tag{5}$$

Thus, the orographic precipitation is determined by

$$R = -\mathbf{S}\cdot\int_0^\infty \mathbf{V}\frac{d\rho_{w_s}}{dz}\,dz. \tag{6}$$

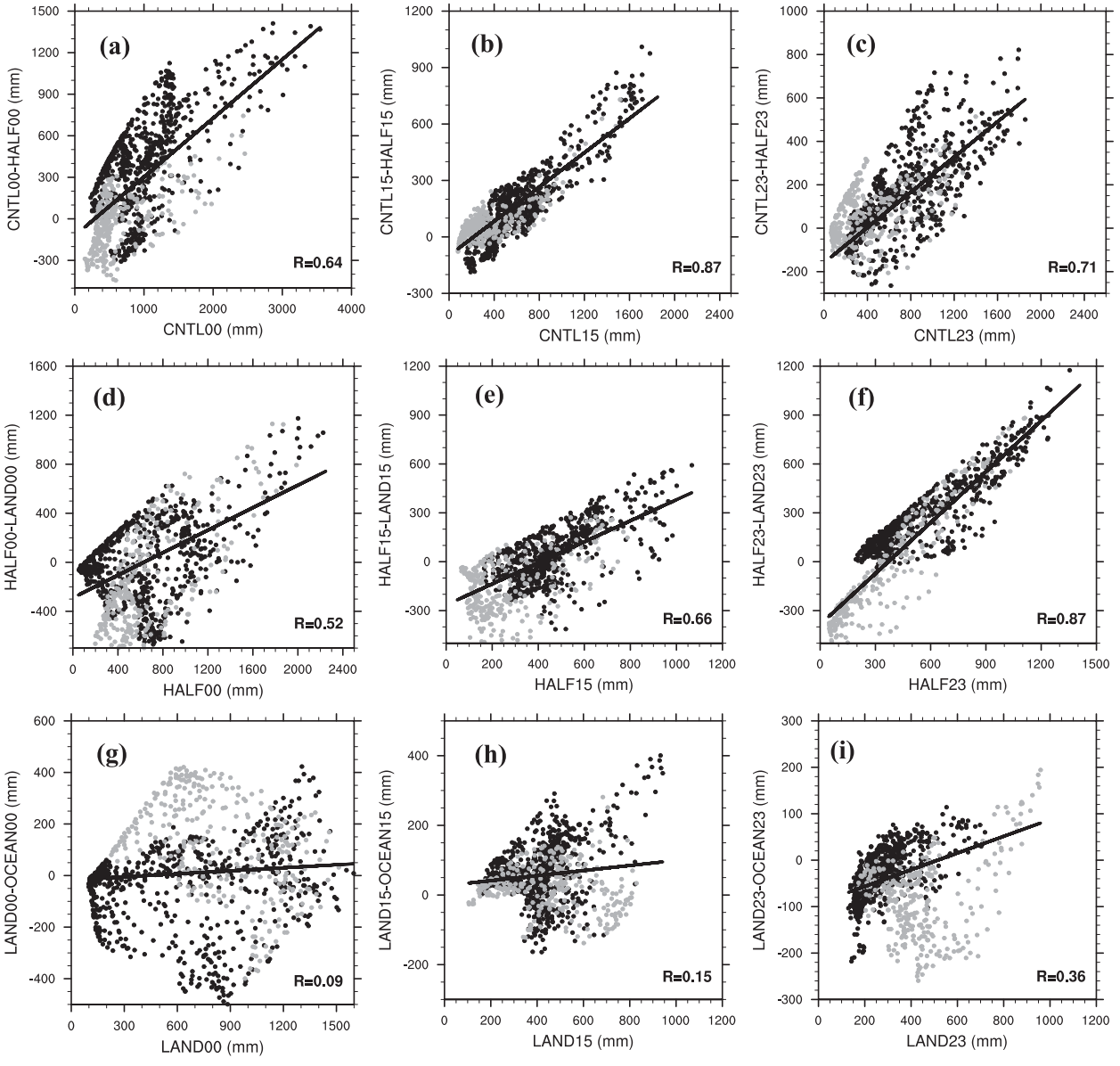

FIG. 10. Scatterplots of 72-h accumulated gridpoint rainfall from CNTL00, CNTL15, and CNTL23 of (a)–(c) CNTL vs CNTL − HALF, (d)–(f) HALF vs HALF − LAND, and (g)–(i) LAND vs LAND − OCEAN. Black solid lines denote the linear regression. Black (gray) dots indicate that the rainfall points are located on the windward (leeward) side of the mountain.

It is seen from (6) that the 1D model of the precipitation is a function of the mountain slope, horizontal wind speed, and water vapor density. The gradient ∇H is interpreted as the lifting effect of the air mass forced from a low elevation to a high elevation when an airstream moves over rising terrain. Meanwhile, the distribution of horizontal wind and water vapor is modified because of the existing mountain.

If the horizontal wind is constant with height and the water vapor tends to be zero at the upper boundary, then (6) would be simplified as

$$R = -\mathbf{S}\cdot\mathbf{V}(\rho_{w_s}) = \mathbf{S}\cdot\mathbf{V}\rho_{w_s}(0) = \mathbf{S}\cdot\mathbf{V}r_s\rho_{\text{air}}(0), \quad (7)$$

where $r_s(0)$ and $\rho_{\text{air}}(0)$ are the saturated water mixing ratio and air density at the surface, respectively. Alpert (1986) used (7) to diagnose the heavy rainfall in the western Mediterranean. Lin et al. (2001), using the method of Doswell et al. (1996), found that the terrain-induced rainfall could explain the main characteristics of the total rainfall in several orographic rainfall events. Similarly, Wu et al. (2002) found that the topography-induced upward motion can be used to estimate the

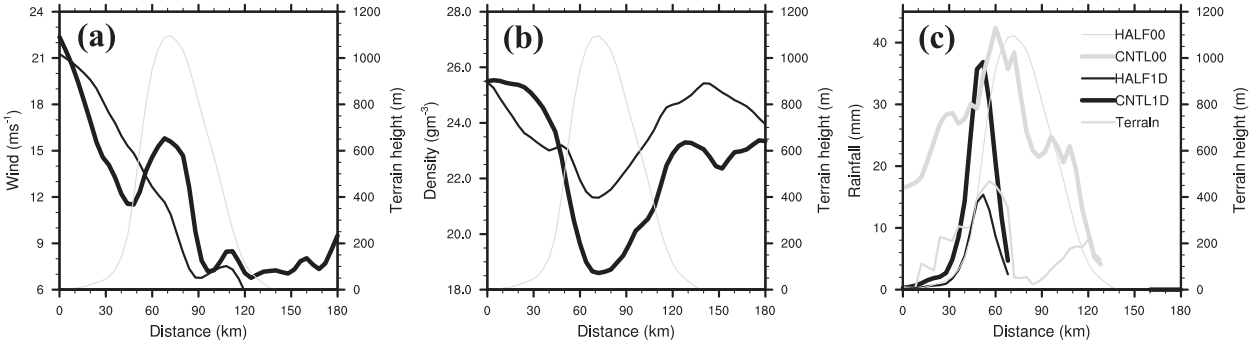

FIG. 11. The meridional mean of (a) surface horizontal wind, (b) water vapor density averaged over the heavy rainfall region, and (c) the 1D model–simulated rainfall of CNTL1D (HALF1D) based on the input from CNTL00 (HALF00). The thick (thin) black lines corresponding with the left axis in (a),(b) denote the variables from CNTL00 (HALF00). The 1-h rainfall of CNTL00 (thick gray line) and HALF00 (thin gray line in (c) is also shown for reference. The thinnest gray lines in each panel indicate the terrain height, which is plotted on the right *y* axis of each panel.

rainfall induced by the mountain range of Taiwan. However, these studies only considered the contribution of the surface wind and water vapor may have underestimated the orographic rainfall. The formula used in these previous studies, which does not vary moisture at different vertical levels, can be considered a simplified form of the 1D model in (3) that is used in this study.

Since the source of moisture for TC rainfall mainly comes from the low to middle levels, only the airflow below 6 km is used to calculate precipitation. The profiles of horizontal wind and water vapor used in the 1D model are the meridional means of the variables over the heavy rainfall region at 0000 UTC 8 August (the results are similar to the 1D analyses at 1200 UTC 8 August; not shown). The WRF forecasted rainfall, along with observational data, is used for comparison while analyzing the 1D model results. Both the WRF and observational meridional mean of the 1-h accumulated rainfall are calculated in the heavy rainfall region from 2300 UTC 7 August to 0000 UTC 8 August. The distributions of surface horizontal wind and water vapor mixing ratio with terrain height in the CNTL00 and HALF00 experiments at 0000 UTC 8 August are shown in Figs. 11a,b. On the windward slope (west) of the mountains, the water vapor mixing ratio and horizontal wind both decrease, while the slope increases with terrain height. The combination of these three ingredients leads to a precipitation maximum at a certain height (between zero and the maximum terrain height). Figure 11c shows that despite a slightly westward bias of the peak location, the 1D model can explain remarkably the upslope rainfall distribution in the WRF model reasonably well, even though it only includes the effects of terrain slope, horizontal wind, and water vapor content. On the other hand, since the mean wind and moisture distribution may vary greatly if the area is located in a different position and distance to the typhoon, the idealized 1D experiments also further highlight the dependence of the heavy precipitation forecast on the accuracy of the track forecast of Morakot.

6. The monsoon–typhoon interaction

The results of the 1D experiment in the previous section show the importance of the mean flow and mid–low-level moisture in controlling the amount of windward precipitation in addition to the apparent impact of the topography through upward lifting. What controls the mean flow toward the mountain ranges and the moisture supplies in southern Taiwan during the heavy rainfall period of Morakot? There is no doubt that the typhoon circulation itself will have a dominant role in driving the westerly winds upslope of the mountains with abundant moisture. On the other hand, during the heavy rainfall period, southern Taiwan is also under the influence of the southwesterly South China Sea monsoon, as can be inferred from Fig. 2a. Most notably, in the South China Sea near the coast of Taiwan, the strong, moist southwest monsoon flow extends into the outer circulation of the TC and impinges upon the southwestern slope of the CMR. There exists an obvious transport of water vapor from the monsoon flow into the TC environment (Fig. 2a). The southwest monsoon is a large-scale system that is believed to have significant impacts on the development of tropical cyclones in the northwest Pacific Ocean (Carr and Elsberry 1995; Briegel and Frank 1997; Chen et al. 2004; Wu et al. 2011).

The influence of the strong southwesterly monsoon circulation on the heavy precipitation associated with Morakot at different temporal and spatial scales has been the subject of several recent studies (e.g., Hong

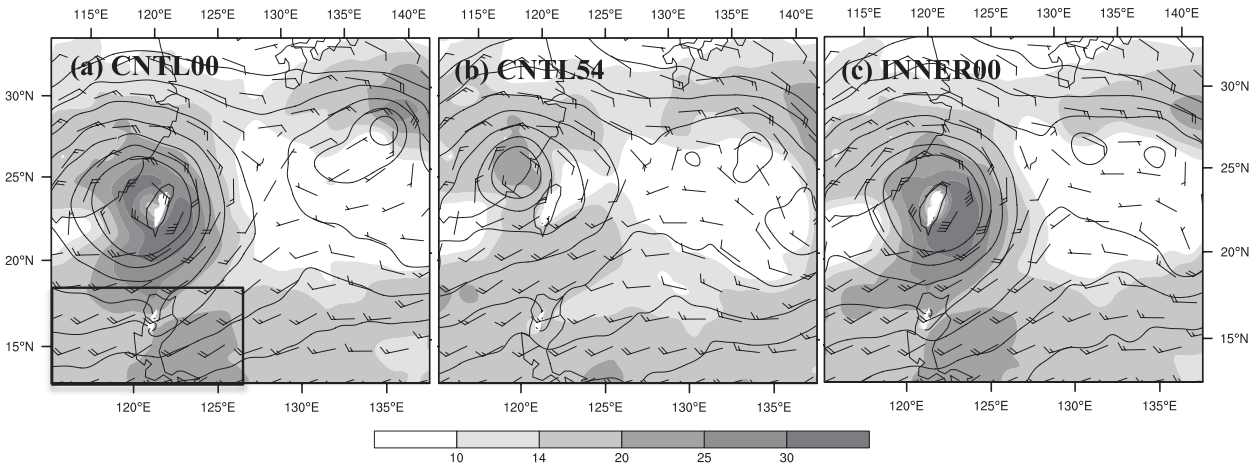

FIG. 12. The 850-hPa wind (full wind barb = 10 m s^{-1}) and height (contour from 1340 to 1460 m by every 20 m) for (a) CNTL00, (b) CNTL54, and (c) INNER00 at 0000 UTC 8 Aug.

et al. 2010; Wu et al. 2011; Lee et al. 2011; Liang et al. 2011; Nguyen and Chen 2011; Chien and Kuo 2011). For example, Wu et al. (2011) showed that Morakot coincided with a quasi-biweekly oscillation and the Madden–Julian oscillation, which enhanced the synoptic-scale southwesterly winds of Morakot and thus decreased its westward movement, leading to a long residence time in the vicinity of Taiwan. The major rainfall area in southern Taiwan is maintained by the monsoon influence, which reduces the translation speed, shifting Morakot northward and enhancing the low-frequency flows on the southern side of the typhoon. Lee et al. (2011) and Chien and Kuo (2011) highlighted the convergence of the typhoon circulation with the monsoon flow as an important factor for creating a quasi-stationary zonal convective band, which induced the heavy rainfall over Taiwan. Nguyen and Chen (2011) documented that the combined circulations associated with the tropical storms and monsoon gyre brought in moisture-laden flows toward the western slopes of southern Taiwan that result in heavy rainfall.

Complementary to the aforementioned studies on the importance of the monsoon circulation, we here present a few unique sensitivity experiments to show the two-way interactions between the typhoon circulation and the southwesterly monsoon flow. It was observed that the low-level monsoon flow to the south of the typhoon circulation during the time of heavy rainfall in CNTL00 (Fig. 12a) is noticeably stronger than that in CNTL54 (Fig. 12b). The typhoon circulation at this time is also noticeably stronger and more to the south (closer to the monsoon flow). On the other hand, the averaged wind speed of the synoptic southerly monsoon flow at 850 hPa is indeed ~1.5 m s^{-1} larger in CNTL00 than in CNTL54 at the initial time (Fig. 13a). In this section, it will be determined whether the difference in the southwesterly flow is primarily due to the difference in the initial monsoon flow between these two simulations, or due to the interaction with the typhoon circulation given the strength and position of the simulated Morakot.

Experiment INNER00 is performed in exactly the same way as CNTL54, except that the initial typhoon circulation within a radius of 600 km measured from the vortex center is replaced by the initial typhoon circulation in CNTL00 within the same radius. The initial monsoon flow in INNER00 by design will be the same as in CNTL54 but weaker than in CNTL00. Interestingly, the INNER00-simulated Morakot follows more or less the same track as in CNTL00 until it makes landfall in Taiwan. Afterward, it turns sharper and more to the north of the track of CNTL00 (Fig. 13b). At 0000 UTC 8 August, the strength and position of the typhoon circulation at 850 hPa (Fig. 12c) are very similar to that of CNTL00 (Fig. 12a) but stronger than in CNTL54 (Fig. 12b) as well as more to the south. Moreover, the monsoon flow to the south of the typhoon circulation in INNER00 is similar to CNTL00, which is stronger than CNTL54 at this time. This evolution can be clearly seen in Fig. 13a, which shows the time evolution of the averaged wind speed of the monsoon flow in the boxed area (denoted in Fig. 12a). Besides a steady increase in all experiments, the monsoon flow strength averaged over the boxed area in INNER00 gradually increases as the typhoon circulation approaches Taiwan Island (Fig. 13a). The average flow matches the strength of CNTRL00 at the initial time, but eventually surpasses CNTRL54 by the end of the simulation. This experiment implies that the strength of the southwesterly monsoon

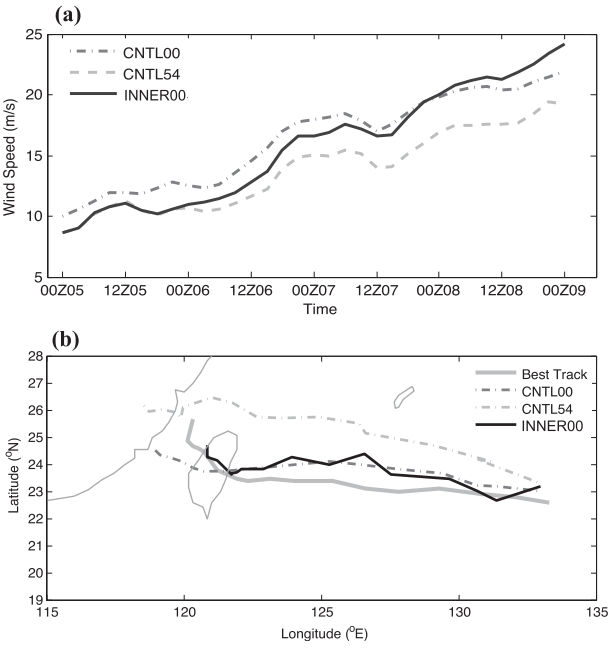

FIG. 13. (a) Mean 850-hPa wind speed of 96-h forecast in the rectangular region shown in Fig. 12a and (b) tracks for CNTL00, CNTL54, and INNER00.

flow can be strongly enhanced by the approaching typhoon circulation, which leads to stronger convergence and moisture transport.

INNER00 also suggests that the track and the strength of the typhoon during the first 72 h of the forecast are mostly controlled by the initial conditions of the typhoon circulation within the 600-km radius rather than by the broader environment. With an improved track, INNER00 also simulates the observed precipitation well, with a maximum concentration in the observed flooding area of southern Taiwan and a peak value of 1936 mm (figure not shown). This has strong implications for observation targeting and observing-system design, which will be the primary subject of another study to be presented elsewhere.

7. Summary and conclusions

As a follow-up to the recent paper on the prediction and predictability of the recent catastrophic flooding event induced by Typhoon Morakot (2009), the current study further utilizes the high-resolution convection-permitting mesoscale ensemble of Z10 but with the addition of numerous sensitivity experiments to explore the impacts of the typhoon track, island topography, and monsoon flow. Consistent with Z10 and complementary to F11, it is found that a good rainfall forecast foremost requires a good track forecast during Morakot's landfall. The dependence of the accuracy of the quantitative precipitation forecast on the track forecast is clearly evident from the high correlation (coefficient = 0.82) between the normalized precipitation error and the storm's center position error among different ensemble members averaged from forecasts before and after landfall time. The influence of the track on rainfall intensity and distribution was further elucidated through two sensitivity experiments that artificially relocated the island topography in the two reference simulations. The rainfall forecast will be greatly degraded if the island is moved away from the typhoon's path (MOVE00 versus CNTL00) while the forecast will improve immensely if the island is relocated to the direct path of the storm (MOVE54 versus CNTL54).

Given a good track forecast, the interaction of the typhoon circulation with complex topography in southern Taiwan plays a dominant role in producing the observed heavy rainfalls. The impacts of the island topography on rainfall intensity and distribution were then examined through a series of sensitivity experiments that differ from the three reference simulations (CNTL00, CNTL15, and CNTL23) by reducing all the island terrain heights by half (the HALF experiments), to flat land at sea level (the LAND experiments), or by removing the land and replacing it with ocean (the OCEAN experiments). These sensitivity experiments show that (i) the presence of Taiwan leads to the redistribution of rainfall from the ocean to the island but does not necessarily extract more total water from the atmosphere, (ii) it is primarily the island topography, not the land interaction, that causes the redistribution of the rainfall, and (iii) the impact of the topography is by no means a linear function of terrain height or terrain slope. Nevertheless, an idealized one-dimensional precipitation-rate forecast model using meridional-mean terrain slope, horizontal wind, and water vapor content from the WRF model, averaged over Taiwan can explain the upslope rainfall distribution remarkably well. Since the mean wind and moisture distribution may vary greatly if the area is located in a different position and distance to the typhoon, the idealized 1D experiments also highlight the dependence of the heavy precipitation forecast on the accuracy of the track forecast of Morakot. Since we used several different realizations of control simulations (CNTL00, CNTL15, and CNTL23) for the WRF and 1D model experiments, one unique aspect of the current study is that the conclusions drawn from various terrain sensitivity experiments are less subject to arbitrary initial conditions or track.

Complementary to recent studies on the importance of the monsoon circulation, our uniquely designed sensitivity experiments show the two-way interactions between the typhoon circulation and the southwesterly

monsoon flow. In particular, it is found that the strength of the southwesterly monsoon gyre could be strongly enhanced by the approaching typhoon circulation, which leads to stronger convergence and moisture transport near Taiwan. These sensitivity experiments show that the interaction between the typhoon and topography, rather than the location of the monsoon flow, contribute the most to the heavy rainfall caused by Morakot. Nevertheless, the presence of the large-scale monsoon background flow remains a crucial factor in producing the rainfall (e.g., Hong et al. 2010; Wu et al. 2011; Lee et al. 2011; Liang et al. 2011; Nguyen and Chen 2011; Chien and Kuo 2011).

Acknowledgments. The first author is sponsored by Graduate Exchange Funds provided by China's Ministry of Education. Proofreading and comments by Thomas Hinson and Erin Munsell are greatly appreciated. This research is partially supported by ONR Grants N000140410471 and N000140910526, a NOAA grant under HFIP, NSF Grant 0840651, and CNSF Grants 40975059 and 40921160380 (awarded to Professor Qinghong Zhang, the first author's home-institute advisor at Peking University). We also acknowledge the Texas Advanced Computing Center (TACC) for computing resources and support.

REFERENCES

Alpert, P., 1986: Mesoscale indexing of the distribution of orographic precipitation over high mountains. *J. Climate Appl. Meteor.,* **25,** 532–545.

Bender, M. A., 1997: The effect of relative flow on the asymmetric structure in the interior of hurricanes. *J. Atmos. Sci.,* **54,** 703–724.

Braun, S. A., and L. Wu, 2007: A numerical study of Hurricane Erin (2001). Part II: Shear and the organization of eyewall vertical motion. *Mon. Wea. Rev.,* **135,** 1179–1194.

Briegel, L. M., and W. M. Frank, 1997: Large-scale influences of tropical cyclogenesis in the western North Pacific. *Mon. Wea. Rev.,* **125,** 1397–1413.

Carr, L. E., III, and R. L. Elsberry, 1995: Monsoon interactions leading to sudden tropical cyclone track changes. *Mon. Wea. Rev.,* **123,** 2295–2318.

Cecil, D. J., 2007: Satellite-derived rain rates in vertically sheared tropical cyclones. *Geophys. Res. Lett.,* **34,** L02811, doi:10.1029/2006GL027942.

Chang, C.-P., T.-C. Yeh, and J. M. Chen, 1993: Effects of terrain on the surface structure of typhoons over Taiwan. *Mon. Wea. Rev.,* **121,** 734–752.

Chang, S. M., 1982: The orographic effect induced by an island mountain range on propagating tropical cyclones. *Mon. Wea. Rev.,* **110,** 1255–1270.

Chen, T.-C., S.-Y. Wang, M.-C. Yen, and W. A. Gallus Jr., 2004: Role of the monsoon gyre in the interannual variation of tropical cyclone formation over the western North Pacific. *Wea. Forecasting,* **19,** 776–785.

Chiao, S., and Y.-L. Lin, 2003: Numerical modeling of an orographically enhanced precipitation event associated with Tropical Storm Rachel over Taiwan. *Wea. Forecasting,* **18,** 325–344.

Chien, F.-C., and H.-C. Kuo, 2011: On the extreme rainfall of Typhoon Morakot (2009). *J. Geophys. Res.,* **116,** D05104, doi:10.1029/2010JD015092.

Corbosiero, K. L., and J. Molinari, 2002: The effects of vertical wind shear on the distribution of convection in tropical cyclones. *Mon. Wea. Rev.,* **130,** 2110–2123.

——, and ——, 2003: The relationship between storm motion, vertical wind shear, and convective asymmetries in tropical cyclones. *J. Atmos. Sci.,* **60,** 366–376.

Doswell, C. A., III, H. Brooks, and R. Maddox, 1996: Flash flood forecasting: An ingredient-based methodology. *Wea. Forecasting,* **11,** 560–581.

Fang, X., Y.-H. Kuo, and A. Wang, 2011: The impact of Taiwan topography on the predictability of Typhoon Morakot's record-breaking rainfall: A high-resolution ensemble simulation. *Wea. Forecasting,* **26,** 613–633.

Frank, W. M., and E. A. Ritchie, 1999: Effects of environmental flow upon tropical cyclone structure. *Mon. Wea. Rev.,* **127,** 2044–2061.

Gao, S., Z. Meng, F. Zhang, and L. F. Bosart, 2009: Torrential rainfall mechanisms of severe Tropical Storm Bilis (2006) after its landfall: Observational analysis. *Mon. Wea. Rev.,* **137,** 1881–1897.

Ge, X., T. Li, S. Zhang, and M. Peng, 2010: What causes the extremely heavy rainfall in Taiwan during Typhoon Morakot (2009)? *Atmos. Sci. Lett.,* **11,** 46–50.

Hong, C.-C., H.-H. Hsu, M.-Y. Lee, and J.-L. Kuo, 2010: Role of submonthly disturbance and 40-50-day ISO on the extreme rainfall event associated with Typhoon Morakot (2009) in Southern Taiwan. *Geophys. Res. Lett.,* **37,** L08805, doi:10.1029/2010GL042761.

Hong, S.-Y., and J.-O. J. Lim, 2006: The WRF Single-Moment 6-class Microphysics scheme (WSM6). *J. Korean Meteor. Soc.,* **42,** 129–151.

Jian, G.-J., and C.-C. Wu, 2008: A numerical study of the track deflection of Supertyphoon Haitang (2005) prior to its landfall in Taiwan. *Mon. Wea. Rev.,* **136,** 598–615.

Kuo, Y.-H., and W. Wang, 1997: Rainfall prediction of Typhoon Herb with a mesoscale model. Preprints, *Workshop on Typhoon Research in the Taiwan Area,* Boulder, CO, National Science Council, 35–45.

Lee, C.-S., C.-C. Wu, T.-C. C. Wang, and R. L. Elsberry, 2011: Advances in understanding the ''Perfect Monsoon-influenced Typhoon'': Summary from International Conference on Typhoon Morakot (2009). *Asia-Pac. J. Atmos. Sci.,* **47,** 213–222.

Liang, J., L. Wu, X. Ge, and C.-C. Wu, 2011: Monsoonal influence on Typhoon Morakot (2009). Part II: Numerical study. *J. Atmos. Sci.,* **68,** 2222–2235.

Lin, Y.-L., 1993: Orographic effects on airflow and mesoscale weather systems over Taiwan. *Terr. Atmos. Oceanic Sci.,* **4,** 381–420.

——, J. Han, D. W. Hamilton, and C.-Y. Huang, 1999: Orographic influence on a drifting cyclone. *J. Atmos. Sci.,* **56,** 534–562.

——, S. Chiao, T.-A. Wang, M. L. Kaplan, and R. P. Weglarz, 2001: Some common ingredients for heavy orographic rainfall. *Wea. Forecasting,* **16,** 633–660.

Nguyen, H. V., and Y.-L. Chen, 2011: High-resolution initialization and simulations of Typhoon Morakot (2009). *Mon. Wea. Rev.,* **139,** 1463–1491.

Skamarock, W. C., J. B. Klemp, J. Dudhia, D. O. Gill, D. M. Barker, W. Wang, and J. G. Powers, 2007: A description of the

advanced research WRF version 2. NCAR Tech. Note NCAR/TN-468+STR, 88 pp.

Smith, R. B., 1979: The influence of mountains on the atmosphere. *Advances in Geophysics,* Vol. 21, Academic Press, 87–230.

Wang, Y., and G. J. Holland, 1996: Tropical cyclone motion and evolution in vertical shear. *J. Atmos. Sci.,* **53,** 3313–3332.

Wu, C.-C., 2001: Numerical simulation of Typhoon Gladys (1994) and its interaction with Taiwan terrain using the GFDL hurricane model. *Mon. Wea. Rev.,* **129,** 1533–1549.

——, and Y.-H. Kuo, 1999: Typhoons affecting Taiwan: Current understanding and future challenges. *Bull. Amer. Meteor. Soc.,* **80,** 67–80.

——, T.-H. Yen, Y.-H. Kuo, and W. Wang, 2002: Rainfall simulation associated with Typhoon Herb (1996) near Taiwan. Part I: The topographic effect. *Wea. Forecasting,* **17,** 1001–1015.

——, K.-W. Cheung, and Y.-Y. Lo, 2009: Numerical study of the rainfall event due to interaction of Typhoon Babs (1998) and the northeasterly monsoon. *Mon. Wea. Rev.,* **137,** 2049–2064.

Wu, L., S. A. Braun, J. Halverson, and G. Heymsfield, 2006: A numerical study of Hurricane Erin (2001). Part I: Model verification and storm evolution. *J. Atmos. Sci.,* **63,** 65–86.

——, J. Liang, and C.-C. Wu, 2011: Monsoonal influence on Typhoon Morakot (2009). Part I: Observational analysis. *J. Atmos. Sci.,* **68,** 2208–2221.

Yeh, T.-C., and R. L. Elsberry, 1993: Interaction of typhoons with the Taiwan orography. Part I: Upstream track deflection. *Mon. Wea. Rev.,* **121,** 3193–3212.

Zhang, F., Y. Weng, Y.-H. Kuo, J. S. Whitaker, and B. Xie, 2010: Predicting Typhoon Morakot's catastrophic rainfall with a convection-permitting mesoscale ensemble system. *Wea. Forecasting,* **25,** 1816–1825.